

Adaptive Measurement Allocation for Learning Kernelized SVMs Under Noisy Observations

Artur Miroszewski

Φ -lab, European Space Agency (ESA/ESRIN), Frascati, Italy

artur.miroszewski@esa.int

Abstract—Kernel methods are typically formulated under the assumption of exact, noise-free access to the Gram matrix. However, in emerging settings such as quantum machine learning, each kernel entry must be inferred from noisy observations, and its accuracy depends on how a limited measurement budget is allocated. Despite this, existing approaches overwhelmingly rely on uniform allocation, which equalizes estimator variance but ignores the highly non-uniform dependence of kernelized classifiers on the Gram matrix.

In this work, we introduce an adaptive measurement-allocation strategy for learning kernelized Support Vector Machines (SVMs) from noisy Bernoulli observations. Our approach combines two complementary principles: (i) geometric sensitivity, capturing how perturbations of individual kernel entries affect the classifier margin, and (ii) active-set instability, quantifying the probability of discrete changes in support-vector membership induced by measurement noise. These signals define a task-aware allocation scheme that concentrates measurements on the most decision-critical regions of the kernel matrix.

We provide a theoretical analysis showing that the benefit of adaptive allocation is governed by the heterogeneity of the induced kernel importance structure, leading to distinct regimes in which adaptive or uniform strategies are preferable. Empirical evaluations on synthetic datasets demonstrate that adaptive allocation significantly improves support-vector recovery, margin estimation, and decision-function accuracy under fixed measurement budgets. A dual-coefficient stability criterion further enables early stopping, achieving near-optimal performance while using only a fraction of the measurement cost. Additional experiments on quantum kernels derived from real-world data reveal a regime-dependent behavior aligned with known phenomena such as kernel concentration.

Together, these results establish adaptive measurement allocation as an effective alternative to uniform sampling for learning with noisy kernels, offering improvements in classifier fidelity and overall computational efficiency.

Index Terms—Kernel methods, SVM, adaptive sampling, quantum machine learning, noisy kernels.

I. INTRODUCTION

KERNEL methods [1] are usually presented in a regime where the kernel matrix K is available exactly, up to deterministic numerical precision. In classical settings, each kernel entry $K_{ij} = k(x_i, x_j)$ is computed by evaluating a closed-form function, and its value is treated as noise-free. However, a growing number of modern applications depart fundamentally from this assumption. In such settings, the accuracy of K_{ij} is determined by the number of measurements allocated to its estimation. A prominent example arises in quantum machine learning [2], [3], where kernel entries are estimated from repeated Bernoulli or multinomial shots of

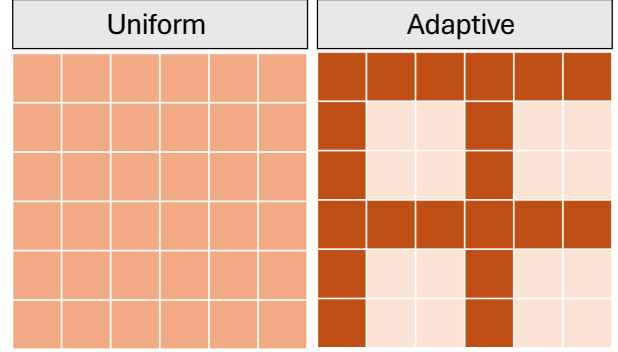


Fig. 1: Conceptual illustration of measurement allocation strategies. The uniform scheme distributes measurement shots evenly across all kernel entries, while our adaptive approach concentrates them in the most influential regions of the kernel, typically involving support vectors and near-margin points, yielding a classifier that more closely matches the true-kernel SVM under the same or smaller measurement budget.

parameterized quantum circuits. Each evaluation of K_{ij} is an empirical, sequential random process, and reducing the variance requires allocating more measurement budget (we use the terms “shots” and “measurements” interchangeably throughout the paper). These challenges become even more pronounced in high-dimensional quantum models, where phenomena such as barren plateaus [4] and kernel concentration [5] can significantly increase the resources required for reliable training [6]. Yet, measurement resources, like experimental shots on a quantum device, are inevitably limited. This creates an unavoidable trade-off: with a fixed global budget, one must decide how to allocate measurements across the independent kernel entries in order to obtain the most accurate downstream classifier.

The standard approach in the literature is uniform sampling, where each kernel entry receives the same number of measurements. Uniform allocation is conceptually simple and symmetric, with well-understood variance properties: it minimizes the maximum variance among the entries and equalizes the per-entry mean-square error. It also ensures that the Frobenius-norm error is evenly spread across the Gram matrix and avoids introducing structural bias. However, uniform allocation is task-agnostic: it treats all entries of the kernel matrix as equally important, despite the fact that downstream learning algorithms rarely depend on the kernel

in a uniform way.

For kernelized SVMs, the dependence of the final classifier on the Gram matrix is highly non-uniform, especially for highly structured problems [1]. Only a small subset of training points, the support vectors, determine the separating hyperplane. These support vectors are identified by the dual solution α , and the influence of a kernel entry K_{ij} on the SVM margin scales proportionally to $\alpha_i \alpha_j y_i y_j$. In the measurement-limited setting, this asymmetry suggests a more efficient strategy: rather than spreading the budget uniformly, one should invest more measurements into those entries that are likely to matter for the support-vector set and the resulting decision boundary.

This structural asymmetry suggests that uniform estimation is inherently suboptimal for SVMs, motivating allocation strategies that explicitly account for the geometry of the learned decision function. Instead of treating kernel estimation as an isolated estimation problem, we view it as part of a learning pipeline whose final goal is to obtain a reliable classifier. Under this perspective, measurement allocation should be guided by indicators of model sensitivity - most importantly, the emerging support vectors and the uncertainty around the decision boundary. This raises several challenges: the support-vector set is unknown early in the process, the kernel estimates are noisy, and sensitivity itself depends on the estimated kernel.

In this work, we introduce an adaptive shot-allocation strategy for learning kernelized SVMs from noisy Bernoulli measurements, grounded in the geometric structure of the SVM solution. The method proceeds in two stages. First, a pilot round collects a modest number of measurements for all kernel entries, providing an initial estimate of the kernel matrix and the corresponding dual coefficients. Subsequently, the algorithm performs a sequence of adaptive rounds, where measurement budget is reallocated according to a score that combines: (i) the sensitivity of the SVM margin to perturbations of individual kernel entries, and (ii) an explicit estimate of active-set instability, capturing the likelihood that points may enter or leave the support-vector set. Together, these signals define a task-aware allocation strategy that focuses resources on the most decision-critical regions of the kernel matrix.

The outcome is a measurement strategy that preferentially refines the kernel entries where accuracy matters most, improving support-vector recovery, margin estimation, and decision-function stability under fixed measurement budgets. Empirically, we observe consistent improvements over uniform allocation in both kernel reconstruction error and classification performance across a range of datasets and noise regimes.

A. Contributions

Our contributions are as follows:

- We formulate measurement allocation for noisy kernel estimation as a task-aware problem tailored to kernelized SVMs, highlighting the non-uniform dependence of the classifier on kernel entries.
- We introduce a novel allocation criterion combining margin sensitivity and active-set instability, providing

an interpretable alternative to gradient-based allocation strategies.

- We develop a multi-round adaptive algorithm that progressively refines kernel estimates in the most influential regions of the Gram matrix.
- We empirically demonstrate that the proposed approach improves support-vector recovery, margin and decision function estimation of the classifier under fixed measurement budgets.

B. Related Work

Quantum kernel methods have emerged as a prominent paradigm for quantum-enhanced machine learning, where similarity between data points is evaluated through overlaps of quantum states [2], [3]. Despite their theoretical appeal, practical deployment remains constrained by the cost of estimating the full Gram matrix, which requires $\mathcal{O}(n^2)$ quantum circuit executions. This challenge is exacerbated in realistic settings by finite-sampling noise, hardware imperfections, and data-acquisition bottlenecks [7].

Recent works have therefore focused on reducing this computational burden. Low-rank approximation techniques, such as Nyström-based methods, have been adapted to quantum kernels to reduce the number of required circuit evaluations while preserving downstream performance [8]. Similarly, kernel matrix completion approaches exploit structural assumptions, such as approximate low-rankness, to infer missing entries and reduce the need for direct quantum measurements [9]. These methods focus primarily on reducing the number of kernel evaluations by exploiting global structure in the Gram matrix.

Shot-efficient quantum kernel learning has also been studied from the perspective of reliability of the downstream classifier. In particular, recent work analyzes how finite-shot noise in kernel entries propagates to the SVM solution and derives bounds on the number of measurements required to preserve the margin and classification performance [10]. These approaches focus on establishing global shot-complexity guarantees under uniform estimation strategies, rather than optimizing the allocation of measurements across individual kernel entries.

More recently, adaptive measurement-allocation strategies have been proposed to distribute shot resources non-uniformly across kernel entries. In particular, a very recent work introduces Adaptive Quantum Kernel Allocation (AQKA) [11], which derives allocation rules from the sensitivity of a global training objective with respect to individual kernel entries. The method leverages gradient-based and KKT-inspired conditions to compute closed-form allocations under a fixed measurement budget, leading to a principled framework grounded in optimal experimental design.

While both AQKA and our approach depart from uniform sampling and exploit the non-uniform relevance of kernel entries, the underlying perspectives differ. AQKA formulates shot allocation as a global optimization problem driven by gradients of a surrogate loss function, whereas our approach focuses specifically on the geometric structure of kernelized SVMs. In particular, we derive allocation signals directly

from the dual coefficients and the stability of the support-vector set, explicitly targeting margin sensitivity and active-set uncertainty. This leads to a simpler and more interpretable allocation mechanism that is tightly coupled to the SVM decision boundary, rather than to a generic objective function.

Orthogonally to kernel estimation, recent work has investigated the computational complexity of inference in quantum kernel methods. In particular, [12] shows that by encoding the full decision function as a single observable and employing quantum amplitude estimation, the query complexity of inference can be reduced from $\mathcal{O}(N)$ to $\mathcal{O}(|\alpha|_1/\epsilon)$, which is provably optimal. These results address the cost of evaluating trained models, and are complementary to our focus on shot-efficient estimation of the kernel matrix itself.

C. Manuscript structure

The remainder of the paper is organized as follows. In Section II, we introduce the measurement model and review the formulation of kernelized SVMs under noisy kernel estimates. Section III presents our analysis of sensitivity and support-vector structure, which forms the basis for task-aware measurement allocation. In Section IV, we describe the proposed adaptive shot-allocation algorithm. Section V reports numerical experiments evaluating kernel reconstruction, classifier stability, and predictive performance. Finally, Section VI concludes with a discussion of limitations and future directions.

II. BACKGROUND

A. Support Vector Machines

Support Vector Machines (SVMs) are large-margin classifiers that construct a decision function by focusing on the most informative training points, known as *support vectors*. These support vectors lie closest to the decision boundary and fully determine both the geometry of the classifier and its predictive behavior. One of the central strengths of SVMs is that their optimization problem can be expressed entirely in terms of pairwise inner products between data points. This enables the use of *kernels* to implicitly map the data into a high-dimensional feature space without explicitly computing feature embeddings, a mechanism widely known as the *kernel trick*.

Given training samples $\{(x_i, y_i)\}_{i=1}^n$ with labels $y_i \in \{\pm 1\}$ and a positive semidefinite kernel function $K(\cdot, \cdot)$, the SVM is trained by solving the dual optimization problem

$$\begin{aligned} \max_{\alpha} \quad & \sum_{i=1}^n \alpha_i - \frac{1}{2} \sum_{i=1}^n \sum_{j=1}^n \alpha_i \alpha_j y_i y_j K(x_i, x_j), \\ \text{s.t.} \quad & 0 \leq \alpha_i \leq C, \quad \sum_{i=1}^n \alpha_i y_i = 0, \end{aligned} \quad (1)$$

where the variables α_i are the *dual coefficients*. These coefficients measure the contribution of each training sample to the decision boundary. At optimality, only a subset of coefficients satisfies $\alpha_i > 0$; the associated samples constitute the support vectors. Because the dual formulation depends exclusively on $K(x_i, x_j)$, the SVM directly incorporates similarities between samples without requiring explicit feature representations.

Once the optimal coefficients α are obtained, the decision function takes the form

$$f(x) = \sum_{i=1}^n \alpha_i y_i K(x_i, x) + b, \quad (2)$$

where b is the bias recovered from the Karush–Kuhn–Tucker conditions. The signed distance to the decision boundary is given by $f(x)$, and classification is determined by $\text{sign}(f(x))$.

The margin of the classifier $1/\|w\|$ quantifies the separation between the two classes. The norm can be expressed in terms of the dual variables as

$$\|w\| = \sqrt{\sum_{i,j} (\alpha_i y_i) K_{ij} (\alpha_j y_j)}. \quad (3)$$

Because both the decision function and the geometry of the separating hyperplane depend on the kernel only through weighted combinations involving the dual coefficients, perturbations in different kernel entries have highly non-uniform effects on the learned classifier. In particular, entries associated with support vectors and near-margin samples dominate both the margin and the decision function, while perturbations involving non-support vectors have negligible first-order impact. This structural sparsity of the SVM solution implies that kernel estimation is inherently task-dependent, with certain regions of the Gram matrix playing a disproportionately important role. This observation forms the basis for the adaptive allocation strategies developed in this work.

B. Measurement-Based Kernels

Let $K \in [0, 1]^{n \times n}$ denote the true, symmetric, positive semi-definite kernel matrix and assume for simplicity that the kernel is normalized such that $K_{ii} = 1$. In practice, the learner does not have direct access to the entries K_{ij} , but instead accesses kernel entries through a stochastic measurement procedure, in which noisy realizations of the kernel are prepared and sampled.

The effective kernel values are intended to approximate the true kernel, but may be impacted by hardware noise, as is typical in near-term quantum computing devices [13], [14]. We model this by introducing a stochastic effective kernel process $K^{(t)}$, where each realization corresponds to one execution of the underlying kernel-evaluation procedure:

$$K^{(k)} = K + \varepsilon^{(k)}, \quad (4)$$

where the noise term $\varepsilon^{(k)}$ represents hardware-induced fluctuations satisfying

$$\mathbb{E}[\varepsilon^{(k)}] = 0. \quad (5)$$

We do not assume that the noise realizations $\varepsilon^{(k)}$ are independent across measurement shots. In particular, correlations between $\varepsilon^{(k)}$ and $\varepsilon^{(s)}$ for $k \neq s$ are allowed, capturing realistic effects such as calibration drift, coherent errors, or slowly varying hardware fluctuations. Define (for $k \neq s$)

$$\sigma_{\text{phys},ij}^2 := \text{Cov}(K_{ij}^{(k)}, K_{ij}^{(s)}), \quad k \neq s, \quad (6)$$

where we assume that the kernel noise process admits finite second moments and stationary second-order statistics, i.e.

$\text{Cov}(K_{ij}^{(t)}, K_{ij}^{(s)})$ depends only on whether $t = s$ or $t \neq s$. As we will see, these correlations induce variability in the effective kernel across repeated evaluations that cannot be reduced by averaging alone.

Given a realization of the effective kernel, individual measurements are obtained through Bernoulli sampling:

$$X_{ij}^{(k)} \sim \text{Bernoulli}(K_{ij}^{(k)}), \quad k = 1, \dots, N_{ij}, \quad (7)$$

where N_{ij} is the number of measurement shots allocated to the pair (i, j) . The empirical estimator

$$\widehat{K}_{ij} = \frac{1}{N_{ij}} \sum_{k=1}^{N_{ij}} X_{ij}^{(k)} \quad (8)$$

is an unbiased estimator of the mean effective kernel,

$$\mathbb{E}[\widehat{K}_{ij}] = K_{ij} \quad (9)$$

which follows from the zero-mean assumption on the noise. This formulation separates two distinct sources of uncertainty: variability in the kernel itself, captured by $\varepsilon^{(k)}$, and sampling noise arising from finite-shot measurements.

The variance of the estimator reflects two distinct sources of uncertainty: finite-shot sampling noise and fluctuations of the underlying kernel across repeated evaluations (See App. A),

$$\text{Var}(\widehat{K}_{ij}) = \frac{K_{ij}(1 - K_{ij})}{N_{ij}} + \left(1 - \frac{1}{N_{ij}}\right) \sigma_{\text{phys},ij}^2. \quad (10)$$

The first term corresponds to standard binomial sampling noise and decreases with N_{ij} , while the second term represents an irreducible variance component induced by correlations in the underlying kernel process.

The diagonal entries $K_{ii} = 1$ are assumed to be known exactly and require no measurement. Moreover, by symmetry $K_{ij} = K_{ji}$, only the independent kernel entries in the upper triangle (excluding the diagonal) must be estimated. We refer to this set as the *independent kernel entries*.

The learner must satisfy a global budget constraint

$$\sum_{1 \leq i < j \leq n} N_{ij} = N_{\text{tot}}, \quad (11)$$

which limits the total number of measurements across kernel entries. Crucially, the variance of \widehat{K}_{ij} depends on both the allocation N_{ij} and the intrinsic noise level $\sigma_{\text{phys},ij}^2$, making the estimation problem inherently heterogeneous across entries. Since different kernel entries contribute unequally to the downstream SVM solution, this heterogeneity suggests that uniform measurement strategies are generally suboptimal, and motivates adaptive allocation schemes that prioritize the most informative regions of the kernel matrix.

C. Sensitivity of the SVM to Kernel Perturbations

In the measurement-based setting, the learner controls the accuracy of individual kernel entries \widehat{K}_{ij} only through the allocated number of Bernoulli shots N_{ij} . Because each kernel entry enters the dual objective explicitly, even small perturbations of particular kernel values can alter the learned classifier. In this subsection we examine how the SVM solution responds to changes in K_{ij} , focusing on its two geometric

components: the margin $\|w\|$ and the decision function $f(x)$. Importantly, these sensitivities exhibit a highly structured and sparse pattern, reflecting the geometry of the SVM solution rather than a global dependence on all kernel entries.

When a small perturbation δK_{ij} does not change the identity of the active set (i.e., the indices corresponding to $\alpha_i = 0$, $0 < \alpha_i < C$, and $\alpha_i = C$ remain unchanged), the optimal dual variables α can be treated as locally constant. Under this condition, the envelope theorem (See App. B) implies that the derivative of the margin with respect to a kernel entry is the partial derivative of the dual objective evaluated at the optimum, without differentiating through α .

This yields a clean expression:

$$\frac{\partial \|w\|^2}{\partial K_{ij}} = \alpha_i \alpha_j y_i y_j. \quad (12)$$

Thus the influence of K_{ij} on the classifier geometry is determined by:

- whether both i and j are support vectors,
- the magnitude of their dual coefficients,
- and the label interaction term $y_i y_j$.

Kernel entries involving non-support vectors ($\alpha_i = 0$ or $\alpha_j = 0$) have zero first-order influence on the margin. This reveals a strong sparsity structure: only a small subset of kernel entries, those associated with active constraints, contribute meaningfully to the geometry of the classifier.

D. Active-Set Instability and Near-Margin Uncertainty

Support Vector Machines depend not only on the numerical values of the dual coefficients, but also critically on the identity of the indices that satisfy the optimality conditions. This set of indices constitutes the active set (the support vectors). In the process of kernel estimation changes in the kernel matrix can alter the margin geometry and the decision values, potentially causing a point to enter or leave the support-vector set. Because measurement noise affects \widehat{K} unevenly across entries, the risk of these active-set transitions is non-uniform across training points. Additionally, unlike smooth variations in the dual variables, changes in this active set constitute discrete transitions that can significantly alter the classifier.

In the context of kernel estimation, perturbations in the kernel matrix modify both the margin geometry and the decision values, potentially causing a point to enter or leave the support-vector set. At the optimum, each point satisfies one of the complementary slackness conditions:

$$\begin{cases} \alpha_i = 0, & y_i f(x_i) > 1, \\ 0 < \alpha_i < C, & y_i f(x_i) = 1, \\ \alpha_i = C, & y_i f(x_i) < 1. \end{cases} \quad (13)$$

Thus, changes in support-vector membership correspond to threshold-crossing events in the margin residual

$$\Delta_i = y_i f(x_i) - 1. \quad (14)$$

If

- $\Delta_i > 0$, the point lies outside the margin and has $\alpha_i = 0$,
- $\Delta_i = 0$, the point lies exactly on the margin, with $0 < \alpha_i < C$,

- $\Delta_i < 0$, the soft-margin constraint is active, yielding $\alpha_i = C$.

Noise (hardware or measurement) perturbs the decision values $f(x_i)$, so the sign of Δ_i becomes uncertain whenever the decision function is uncertain. Points with small $|\Delta_i|$ lie close to the decision boundary and are therefore most susceptible to changes in support-vector status under perturbations.

From the measurement model, each entry K_{ij} has variance given in Eq. 10. Since the decision function, Eq. 2, is linear in the kernel entries, its variance under measurement noise is

$$\sigma_{f,i}^2 = \text{Var}(\hat{f}(x_i)) = \sum_{j=1}^n (\hat{\alpha}_j y_j)^2 \text{Var}(\hat{K}_{ij}) \quad (15)$$

A perturbation in $f(x_i)$ causes a change of support-vector status if the perturbed value crosses the margin threshold. A simple and effective approximation is obtained by treating the decision value as locally Gaussian,

$$f(x_i) \approx \hat{f}(x_i) + \mathcal{N}(0, \sigma_{f,i}^2). \quad (16)$$

This approximation is justified by the aggregation of multiple independent or weakly correlated noise contributions in the decision function. Under this approximation, the probability that x_i lies on the margin (or inside it) is

$$P_i := \mathbb{P}(y_i \hat{f}(x_i) \leq 1) = \Phi\left(-\frac{\hat{\Delta}_i}{\sigma_{f,i}}\right), \quad (17)$$

where $\hat{\Delta}_i = y_i \hat{f}(x_i) - 1$ is the plug-in margin residual based on the current estimated kernel \hat{K} , and Φ is the standard normal CDF. The quantity P_i can be interpreted as the probability that the point x_i lies on or within the margin under measurement noise, and therefore as a proxy for the likelihood that x_i belongs to, or may transition into, the support-vector set.

This perspective reveals a second, fundamentally different source of sensitivity beyond the local derivatives discussed earlier. While gradient-based sensitivity captures how the objective varies under infinitesimal perturbations, active-set instability captures discrete structural changes in the classifier induced by finite perturbations. As a result, points with high transition probability P_i represent regions where additional measurement precision is most valuable, as errors in these regions can alter both the composition of the support-vector set and the resulting decision boundary.

III. PROBLEM FORMULATION AND MEASUREMENT STRATEGIES

A. Problem Formulation

Let $K \in [0, 1]^{n \times n}$ denote the true positive-semidefinite kernel matrix and let α , $f(\cdot)$, $\|w\|$ be the corresponding SVM solution obtained from (1). This “true-kernel SVM” serves as the reference model.

In the measurement-based setting, the learner does not have direct access to the exact entries of K . Instead, the off-diagonal coefficients are estimated sequentially through Bernoulli measurements. After N_{ij} measurements, the learner obtains an estimate \hat{K}_{ij} (Eq. 8), whose variance decreases as $\mathcal{O}(1/N_{ij})$.

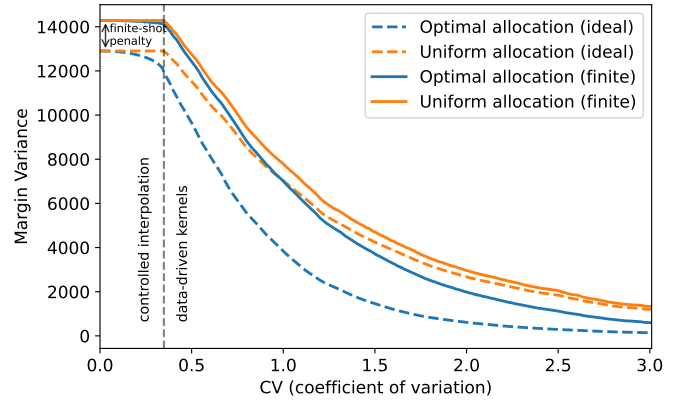


Fig. 2: Variance of uniform and optimal shot-allocation schemes as a function of weight heterogeneity. The top panel shows the margin variance for ideal (dashed) and finite-shot (solid) implementations of optimal and uniform allocation strategies, plotted against the coefficient of variation $\text{std}(w_{ij})/\text{mean}(w_{ij})$. The left region (“controlled interpolation”) is constructed to enforce the homogeneous limit $\text{CV} \rightarrow 0$, where all weights are equal and both allocation schemes coincide. The right region (“data-driven kernels”) corresponds to weights derived from actual kernel instances. As heterogeneity increases, the optimal allocation significantly reduces the variance relative to uniform sampling. Finite-shot effects introduce a systematic upward shift of the optimal curve, most pronounced in the low-CV regime and indicated by the vertical gap between oracle and finite curves (finite-shot penalty), consistent with Eq. 27.

In practice, measurement resources are limited, and we consider a global constraint on the total number of measurements, $\sum_{i < j} N_{ij} = N_{\text{tot}}$ (Eq. 11). Training the SVM on the noisy, progressively refined kernel \hat{K} leads to a model $\hat{\alpha}$, $\hat{f}(\cdot)$, $\|\hat{w}\|$ which generally deviates from the ideal solution. This deviation manifests through multiple mechanisms, including continuous perturbations of the dual coefficients, variations in the margin geometry, fluctuations of decision values, and discrete transitions in

These observations motivate a task-aware formulation of the measurement allocation problem.

Objective. Given a fixed measurement budget N_{tot} , choose measurement counts $\{N_{ij}\}$ to minimize the impact of kernel estimation noise on the learned SVM classifier, subject to the constraint $\sum_{i < j} N_{ij} = N_{\text{tot}}$.

B. Margin Variance Minimization

The objective stated above is conceptually clear but difficult to handle analytically without specifying a concrete measure of degradation of the classifier. Several candidates can be considered, including perturbations of the dual variables, deviations of the decision function, or changes in the geometric margin.

In this work, we focus on minimizing the variance of the squared margin $\|w\|^2$, which provides a global measure of the classifier’s stability and can be directly related to the

kernel matrix through Eq. 3. This choice leads to a tractable approximation in which the effect of measurement noise can be explicitly quantified and optimized.

Importantly, this choice is not unique. Alternative formulations, such as minimizing the variance of the decision function, can be analysed within the same framework. As shown later, these different objectives lead to allocation strategies of similar structure, concentrating measurements on pairs of points associated with large dual coefficients. This consistency justifies the use of margin variance as a representative and analytically convenient surrogate.

To make the objective concrete, we aim to choose measurement counts to solve the constrained problem

$$\min_{\{N_{ij}\}} \text{Var}(\|w\|^2) \quad \text{s.t.} \quad \sum_{i < j} N_{ij} = N_{\text{tot}}. \quad (18)$$

Using the sensitivity result in Eq. 12, we approximate the variance of the squared margin via first-order propagation of kernel estimation errors:

$$\text{Var}(\|w\|^2) \approx \sum_{i < j} (\alpha_i \alpha_j y_i y_j)^2 \text{Var}(\widehat{K}_{ij}). \quad (19)$$

Since $(y_i y_j)^2 = 1$, the label dependence disappears in the squared sensitivity term.

In the presence of both sampling noise and stochastic hardware-induced fluctuations, the variance of the kernel estimator is given by Eq. (10). Substituting this expression yields

$$\begin{aligned} \text{Var}(\|w\|^2) &\approx \\ &\approx \sum_{i < j} (\alpha_i \alpha_j)^2 \left(\frac{K_{ij}(1 - K_{ij})}{N_{ij}} + \left(1 - \frac{1}{N_{ij}}\right) \sigma_{\text{phys},ij}^2 \right). \end{aligned} \quad (20)$$

This expression naturally decomposes into two contributions:

$$V_{\text{sampling}} = \sum_{i < j} (\alpha_i \alpha_j)^2 \frac{K_{ij}(1 - K_{ij})}{N_{ij}}, \quad (21)$$

$$V_{\text{phys}} = \sum_{i < j} (\alpha_i \alpha_j)^2 \sigma_{\text{phys},ij}^2. \quad (22)$$

The term V_{sampling} corresponds to variance arising from finite sampling and can be reduced by increasing the number of measurements. In contrast, V_{phys} captures the contribution of correlated kernel fluctuations and constitutes an irreducible variance component that is independent of the allocation strategy.

The optimization problem therefore reduces to minimizing V_{sampling} under the budget constraint, since V_{phys} does not depend on $\{N_{ij}\}$. This leads to the optimal allocation (See App. C):

$$N_{ij}^* = N_{\text{tot}} \frac{\sqrt{w_{ij}}}{\sum_{k < l} \sqrt{w_{kl}}}, \quad (23)$$

where

$$w_{ij} = (\alpha_i \alpha_j)^2 K_{ij}(1 - K_{ij}). \quad (24)$$

The weights w_{ij} quantify the contribution of each kernel entry to the variance of the margin, combining both sensitivity (through $\alpha_i \alpha_j$) and intrinsic estimation difficulty (through $K_{ij}(1 - K_{ij})$).

Thus, the presence of hardware-induced kernel fluctuations does not alter the structure of the optimal allocation, but introduces a fundamental limit on the achievable accuracy of the estimator. In particular,

$$\lim_{N_{\text{tot}} \rightarrow \infty} \text{Var}(\|w\|^2) = \sum_{i < j} (\alpha_i \alpha_j)^2 \sigma_{\text{phys},ij}^2, \quad (25)$$

showing that the variance cannot be reduced below a hardware-imposed floor.

The above allocation expression characterizes an idealized optimum, assuming oracle access to the true kernel and the associated optimal dual solution, and thus to the weights w_{ij} . In practice, these quantities must be estimated from noisy measurements. We therefore proceed by relaxing this idealized setting, first by enforcing discrete shot allocations and subsequently by incorporating uncertainty in the learned classifier into the allocation strategy, capturing both sensitivity and uncertainty effects.

C. Comparison with Uniform Allocation

A natural baseline for estimating the kernel matrix under a finite measurement budget is the *uniform measurement scheme*, in which the total budget N_{tot} is distributed evenly across all independent off-diagonal kernel entries. Each pair (i, j) with $i < j$ receives the same number of measurement shots,

$$N_{ij}^{\text{unif}} = \frac{2N_{\text{tot}}}{n(n-1)}. \quad (26)$$

This approach is currently the most common strategy in practical studies of quantum kernels.

In many works, especially those using classical quantum-circuit simulators such as Qiskit [15] or PennyLane [16], the question of actual measurement cost is often abstracted away: since simulation is deterministic and inexpensive relative to near-term hardware execution, the uniform allocation is adopted by default rather than justified by downstream performance considerations.

For the variance proxy introduced above, Eq. 18, the corresponding variance under uniform allocation is

$$V_{\text{unif}} = \frac{n(n-1)}{2N_{\text{tot}}} \sum_{i < j} w_{ij},$$

while the optimal allocation yields

$$V^* = \frac{\left(\sum_{i < j} \sqrt{w_{ij}}\right)^2}{N_{\text{tot}}}.$$

Proposition 1.

$$V^* \leq V_{\text{unif}},$$

with equality if and only if w_{ij} are constant.

It is important to emphasize that Proposition 1 characterizes an idealized oracle setting, in which the weights w_{ij} are known exactly. In practice, these weights must be estimated from noisy data, and the resulting allocation strategies may deviate from this optimum.

The gap between optimal and uniform allocation is governed by the dispersion of the weights w_{ij} . When the weights are

heterogeneous, the inequality is strict and the optimal allocation, Eq. 23, provides a significant reduction in variance. Since w_{ij} depends on the dual variables, this regime corresponds to structured SVM solutions in which only a subset of training points contributes strongly to the decision boundary.

While the above comparison holds in the ideal case of continuous (fractional) allocations, practical implementations require integer-valued shot counts and rely on estimated weights. As a result, the optimal allocation must be realized through a discrete and noisy approximation, introducing an additional variance penalty. This behavior is illustrated in Fig. 2, which shows the margin variance as a function of weight heterogeneity, quantified by the coefficient of variation $CV = \text{std}(w_{ij})/\text{mean}(w_{ij})$. The dashed curves correspond to ideal allocations, while solid curves represent finite-shot implementations. In the homogeneous regime ($CV \rightarrow 0$), all weights are equal and both strategies coincide, as expected from Proposition 1. However, the finite-shot implementation of the optimal allocation exhibits a slight increase in variance due to fluctuations in the measurement counts, consistent with the analysis below. As heterogeneity increases, the optimal allocation increasingly outperforms uniform allocation, with the gap widening significantly in the high-structure regime.

The following proposition quantifies the effect of deviations from the oracle allocation.

Proposition 2. *Let N_{ij}^* denote the optimal (oracle) allocation given by Eq. 23, and consider a perturbed allocation*

$$N_{ij} = N_{ij}^* + \delta N_{ij},$$

with the constraint $\sum_{i < j} \delta N_{ij} = 0$. Assume that the perturbations δN_{ij} are small.

Then, under a second-order Taylor expansion of the variance objective, the expected increase in the variance satisfies

$$\mathbb{E}[V] = V^* + \sum_{i < j} \frac{w_{ij}}{(N_{ij}^*)^3} \mathbb{E}[(\delta N_{ij})^2] + \mathcal{O}(\|\delta N\|^3). \quad (27)$$

- The optimal allocation derived above does not explicitly account for the integer nature of measurement shots. In practice, shot counts must be integer-valued, which introduces deviations from the ideal allocation, captured by the perturbations δN_{ij} . Proposition 2 shows that such deviations lead to a systematic increase in the variance due to the convex dependence on $1/N_{ij}$. This effect manifests as an upward shift in the variance of both uniform and optimal allocation strategies, as observed in Fig. 2. The magnitude of this shift depends on the distribution of N_{ij}^* and is typically more pronounced when the optimal allocation assigns small measurement counts to a subset of entries.
- The oracle allocation assumes access to the exact weights w_{ij} , while in practice these weights must be inferred from noisy kernel estimates and intermediate models. This introduces an additional source of error not present in uniform allocation, as inaccuracies in the estimated weights lead to misallocation of measurement effort. As a result, in regimes where the underlying structure is weak (i.e., w_{ij} are nearly homogeneous), these estimation

errors can dominate the benefits of adaptivity, and uniform allocation may outperform adaptive strategies. This defines a regime of *uniform superiority* in low-structure settings.

Taken together, these results reveal a three-regime behavior of measurement allocation strategies. In highly structured settings, where the weights w_{ij} are strongly heterogeneous, the optimal allocation provides substantial gains over uniform sampling, even in the presence of discretization and estimation noise. In moderately structured regimes, these gains persist but are partially reduced by implementation effects. In contrast, in low-structure regimes where the kernel contributions are nearly uniform, the benefits of adaptivity diminish and can be outweighed by errors in weight estimation, making uniform allocation preferable due to its robustness. This transition between regimes is explored empirically in Section V and in Fig. 8

D. Decision Function Variance Minimization

While the previous analysis focused on the variance of the margin, one may alternatively consider minimizing the variance of the decision function. Recall that the decision value at a training point x_i is given by Eq. 2. Under the same noise model, the variance of $f(x_i)$ can be approximated as in Eq. 15. Aggregating the variance over all training points provides a global objective measuring decision-function stability

$$V_{\text{dec}} = \sum_{i < j} (\alpha_i^2 + \alpha_j^2) \frac{K_{ij}(1 - K_{ij})}{N_{ij}},$$

which corresponds to weights

$$w_{ij}^{\text{dec}} := (\alpha_i^2 + \alpha_j^2) K_{ij}(1 - K_{ij}),$$

The allocation derived from margin variance minimization (Eq. 23) is given by

$$N_{ij}^{\text{margin}} \propto |\alpha_i \alpha_j| \sqrt{K_{ij}(1 - K_{ij})},$$

while the decision-based allocation scales as

$$N_{ij}^{\text{dec}} \propto \sqrt{\alpha_i^2 + \alpha_j^2} \sqrt{K_{ij}(1 - K_{ij})}.$$

Although these expressions differ in their exact dependence on the dual variables, they exhibit the same qualitative behavior. In particular, both allocations assign larger budgets to entries involving large dual coefficients, and therefore concentrate measurements on support vectors. Moreover, by standard inequalities,

$$|\alpha_i \alpha_j| \leq \frac{1}{2}(\alpha_i^2 + \alpha_j^2) \leq \alpha_i^2 + \alpha_j^2,$$

the two weighting schemes are comparable up to constant factors, implying that both induce similar allocation patterns.

Therefore, both objectives lead to allocation strategies that exploit the same underlying geometric structure of the SVM solution. This demonstrates that the specific choice of margin variance as the optimization target is not restrictive, but rather representative of a broader class of objectives that prioritize support-vector regions and near-margin interactions. Consequently, the heterogeneity effects and performance trade-offs discussed in the previous subsection carry over directly to alternative formulations based on decision-function stability.

IV. ADAPTIVE MEASUREMENT ALLOCATION

A. Adaptive Allocation Algorithm Overview

The central idea of our approach is to treat kernel estimation not as an isolated statistical task, but as an integral component of the downstream SVM optimization. In the previous section, we derived an oracle-optimal measurement allocation that minimizes the variance of the classifier under exact knowledge of the kernel and the associated dual solution. In practice, however, this oracle information is unavailable and must be inferred from noisy kernel estimates. The adaptive strategy therefore aims to approximate this ideal allocation in a sequential manner, progressively refining estimates of sensitivity and active-set structure while reallocating measurement effort accordingly. The pseudo code for the algorithm is presented in Algorithm 1 code block and the schematic is presented in Fig. 3. At a high level, the procedure consists of a sequence of measurement–update–retraining cycles:

- 1) **Pilot estimation.** The algorithm begins by allocating a small, uniform number of shots to all independent kernel entries. This pilot phase produces an initial kernel estimate $\widehat{K}^{(0)}$ that is sufficiently accurate to train a first SVM model and extract coarse structural information about the data, in particular the approximate support-vector set and margin geometry. This initial phase is outside the adaptive rounds loop.
- 2) **Sensitivity assessment.** Using the current estimate $\widehat{K}^{(r)}$ and its associated SVM model, the algorithm evaluates *which entries of the kernel matrix matter most* for the classifier. Two complementary and fundamentally different sources of importance are considered:
 - *Geometric sensitivity*
The derivative of $\|w\|^2$ with respect to each kernel entry, capturing first-order geometric sensitivity;
 - *Active-set uncertainty*
The variance of the decision function at each training point, capturing the probability of active-set transitions;
- 3) **Score-based allocation.** These contributions are combined into a single pairwise allocation score s_{ij} for each kernel entry. This score serves as a practical approximation of the oracle weights derived in Section III, augmented with uncertainty information. Higher scores correspond to entries whose improved estimation is expected to stabilize the classifier or reduce variance in margin-critical regions. A portion of the remaining measurement budget is then distributed across entries in proportion to these scores, using a multinomial sampling step to ensure integer shot counts.
- 4) **Kernel update and model retraining.** After allocating new shots, the kernel estimate is updated to $\widehat{K}^{(r+1)}$. A new SVM is trained on this updated kernel, providing refined dual coefficients, a more accurate set of margin-critical points, and improved estimates of the decision-value variances.
- 5) **Early-stopping mechanism.** The iteration continues until the total budget is utilized or the early-stopping

Algorithm 1 Adaptive Measurement Allocation for Kernelized SVMs

- 1: **Input:** $\{(x_i, y_i)\}_{i=1}^n$, budget N_{tot} , rounds R , pilot size m_0 , weight λ , threshold ε
 - 2: **Initialize:** measurement counts $S_{ij} = 0$, $N_{ij} = 0$
 - 3: **Pilot phase:**
 - 4: **for** $i < j$ **do**
 - 5: Draw m_0 shots; update S_{ij} , set $N_{ij} = m_0$
 - 6: $\widehat{K}_{ij} = S_{ij}/N_{ij}$
 - 7: **end for**
 - 8: Train SVM to obtain $\alpha^{(0)}$
 - 9: **for** $r = 1$ to R **do**
 - 10: Compute residuals Δ_i and instability scores P_i
 - 11: $s_{ij} \leftarrow (1 - \lambda)|\alpha_i \alpha_j y_i y_j| + \lambda P_i P_j$
 - 12: $p_{ij} \leftarrow (S_{ij} + 1)/(N_{ij} + 2)$
 - 13: $\text{score}_{ij} \leftarrow s_{ij} \sqrt{p_{ij}(1 - p_{ij})}$
 - 14: Normalize to q_{ij} and allocate shots via multinomial
 - 15: Update S_{ij} , N_{ij} , \widehat{K} and retrain SVM to obtain $\alpha^{(r)}$
 - 16: $\delta_r = \|\alpha^{(r)} - \alpha^{(r-1)}\|/\|\alpha^{(r-1)}\|$
 - 17: **if** $\delta_r < \varepsilon$ **then**
 - 18: **break**
 - 19: **end if**
 - 20: **end for**
 - 21: **return** final \widehat{K} and SVM
-

criterion is met. The criterion is based on dual coefficients stabilization, as measured by the relative change in $y_i \alpha_i$ across successive rounds. This mechanism prevents unnecessary measurements once the classifier has effectively converged, reflecting the fact that further refinement of the kernel has diminishing impact on the SVM solution.

By repeating this loop, the algorithm gradually concentrates measurement effort on the entries that are most influential for the SVM solution. As a result, a substantial portion of the measurement budget is spent where it has the highest impact on classifier accuracy, support-vector recovery, and margin geometry.

This high-level perspective emphasizes the core principle of our method: *allocate measurements where they most improve the learned SVM, rather than where they uniformly reduce kernel estimation error*. This task-aware perspective distinguishes the proposed approach from uniform and purely variance-minimizing strategies, by explicitly linking measurement allocation to classifier sensitivity and structural stability.

B. Pilot Stage and adaptive rounds

The adaptive procedure begins with a **pilot stage**, in which a small and uniformly distributed number of shots is allocated to every independent kernel entry. This stage is effectively a lightweight version of the standard uniform measurement scheme, but with a significantly smaller budget. Its purpose is not to obtain a highly accurate kernel estimate, but rather to produce an initial matrix $\widehat{K}^{(0)}$ that is sufficiently informative to train the first SVM model. The resulting dual coefficients, approximate support-vector set, and preliminary estimates of

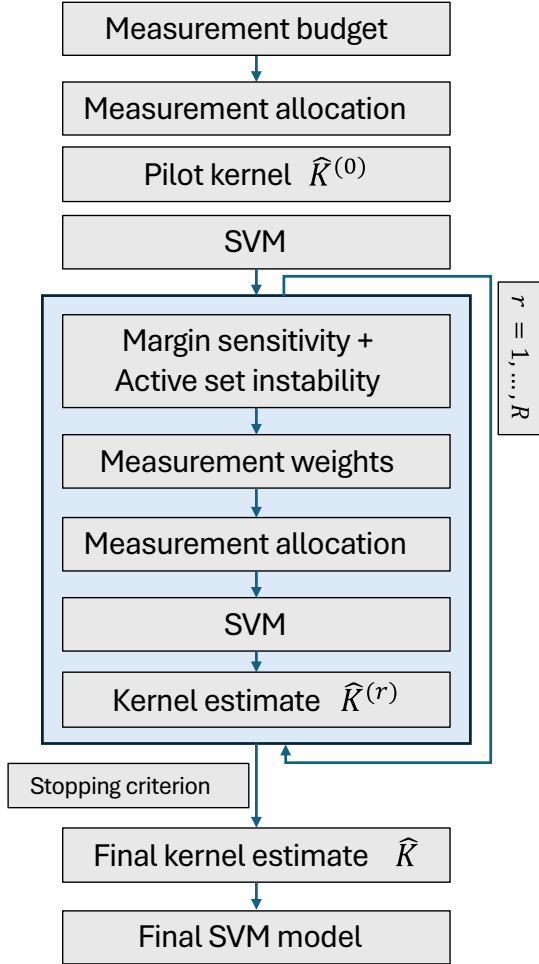


Fig. 3: Schematic overview of the adaptive measurement procedure. A small pilot budget produces an initial kernel estimate, which is used to train a preliminary SVM model. Margin-based sensitivity and active-set instability are combined to assign measurement weights to individual kernel entries. New measurements are allocated accordingly, the kernel estimate is updated, and the process repeats until the stopping criterion is met, yielding a final SVM model closely matching the true-kernel solution.

margin proximity form the initial “sense” of the classifier geometry that guides all subsequent rounds.

Each **adaptive round** refines the kernel estimate by directing additional measurement shots toward entries that the current SVM model identifies as most influential. The allocation is governed by two complementary signals:

a) *Margin sensitivity*: The derivative $\partial\|w\|^2/\partial K_{ij}$ defined in (12) quantifies how strongly a perturbation of the entry K_{ij} affects the classifier’s margin. Large values correspond to pairs of points with high dual coefficients, and therefore identify kernel entries whose perturbations induce the largest first-order changes in the classifier geometry.

b) *Active-set instability*: The probability P_i that point i is effectively at risk of becoming (or ceasing to be) a support vector, as defined in (17), captures the probability that uncertainty in the decision value induces a change in support-vector status.

Since such changes correspond to discrete transitions in the classifier structure, the joint term $P_i P_j$ identifies kernel entries whose noise may trigger simultaneous active-set changes in multiple margin-critical points.

These effects are combined into the pairwise allocation weight

$$s_{ij} = (1 - \lambda) |\alpha_i \alpha_j y_i y_j| + \lambda P_i P_j C^2, \quad (28)$$

where $\lambda \in [0, 1]$ controls the relative importance of geometric sensitivity and active-set uncertainty and the factor C^2 ensures that the active-set instability term is scaled consistently with the maximum possible contribution of support vectors, whose dual coefficients lie in $[0, C]$. Following the theoretical allocation derived in the previous section, these scores are further modulated by the Bernoulli variance term $p_{ij}(1 - p_{ij})$, where p_{ij} is the current estimate of K_{ij} , prioritizing entries whose estimates remain statistically uncertain. This score can be interpreted as a practical approximation of the oracle weights derived in Section III, augmented by uncertainty-aware terms capturing active-set instability. A portion of the remaining budget is then allocated across independent entries according to these scores via a multinomial draw to obtain integer shot counts. After the new measurements are taken, the kernel estimator \hat{K} is updated and a fresh SVM model is trained. This iterative refinement causes the allocation to progressively concentrate on a small subset of kernel entries associated with stable support vectors and near-margin points, mirroring the structure of the oracle-optimal allocation as the kernel estimate converges.

C. Stopping criterion

The adaptive procedure iteratively refines the kernel estimate and retrains the SVM after each measurement round. The stopping mechanism is triggered either when the measurement budget is exhausted or when the learned classifier has effectively converged. To detect convergence, we monitor the stability of the dual coefficients. Since both the SVM decision function and the margin depend only on the quantity $y_i \alpha_i$, stabilization of this vector provides a principled proxy for convergence of the classifier. In particular, changes in $y_i \alpha_i$ directly translate into changes in both the decision boundary and the margin geometry.

Let $\alpha^{(r)}$ denote the dual coefficients obtained after round r , and similarly $\alpha^{(r-1)}$ those of the previous round. We define the relative change between successive iterates as

$$\delta^{(r)} = \frac{\|\alpha^{(r)} - \alpha^{(r-1)}\|_2}{\|\alpha^{(r-1)}\|_2 + 10^{-12}}. \quad (29)$$

The small denominator offset prevents numerical issues when the dual coefficients are close to zero in early rounds. When this relative change falls below a prescribed tolerance, $\delta^{(r)} < \varepsilon$, we conclude that further measurements are unlikely to significantly affect the classifier. At this stage, additional refinement of the kernel matrix has diminishing impact on both the decision function and the margin, and the algorithm terminates early.

If instead the dual coefficients continue to change appreciably, the procedure proceeds to the next round, allocating additional measurements based on the updated sensitivity and instability estimates. This adaptive stopping criterion ensures that measurement effort is not wasted once the classifier has stabilized.

D. Quantum–Classical Cost Comparison and Practical Regimes

To compare the efficiency of adaptive and uniform measurement strategies, we model the total computational cost as the sum of a quantum component, proportional to the number of measurement shots, and a classical component, dominated by retraining the SVM.

The quantum cost scales proportionally with the total number of measurements, $c_q N_{\text{tot}}$, while the classical cost scales as $c_c(R+1)n^3$, reflecting the worst-case complexity of solving the dual SVM problem with a dense kernel matrix [17]. An adaptive scheme performing one pilot and R refinement rounds therefore requires $R+1$ SVM trainings, while the uniform scheme performs a single training.

The total costs are given by

$$\begin{aligned} C_{\text{uniform}} &= c_q N_{\text{tot}} + c_c n^3, \\ C_{\text{adaptive}} &= c_q r N_{\text{tot}} + (R+1)c_c n^3, \end{aligned}$$

where $r \leq 1$ denotes the fraction of the measurement budget effectively used under early stopping.

To analyze scaling with dataset size, we express the total measurement budget as

$$N_{\text{tot}} = \frac{n(n-1)}{2} \bar{N},$$

where \bar{N} is the average number of measurements per kernel entry.

Introducing the relative cost ratio $\tau = c_c/c_q$, the break-even condition $C_{\text{adaptive}} = C_{\text{uniform}}$ yields a critical value

$$\tau^* = \frac{(n-1)(1-r)}{2n^2 R} \bar{N}. \quad (30)$$

This expression highlights the fundamental trade-off between measurement cost and classical computation. The quantum component scales as $\mathcal{O}(n^2 \bar{N})$, reflecting the number of kernel entries, while the classical component scales as $\mathcal{O}(n^3)$. As a result, adaptive strategies reduce quantum cost by concentrating measurements, but incur additional classical overhead due to repeated model retraining.

The analytical expression above can be interpreted using parameters obtained from the adaptive experiments. In particular, early-stopping results given in Sec. V-D provide realistic values of the effective shot fraction r and the number of refinement rounds R . Figure 4 visualizes the resulting critical values τ^* as a function of dataset size n for representative configurations.

The curves separate regimes in which adaptive or uniform measurement is more cost-efficient. For $\tau < \tau^*$, the reduction in measurement cost achieved by adaptive allocation outweighs the additional retraining overhead, making the adaptive

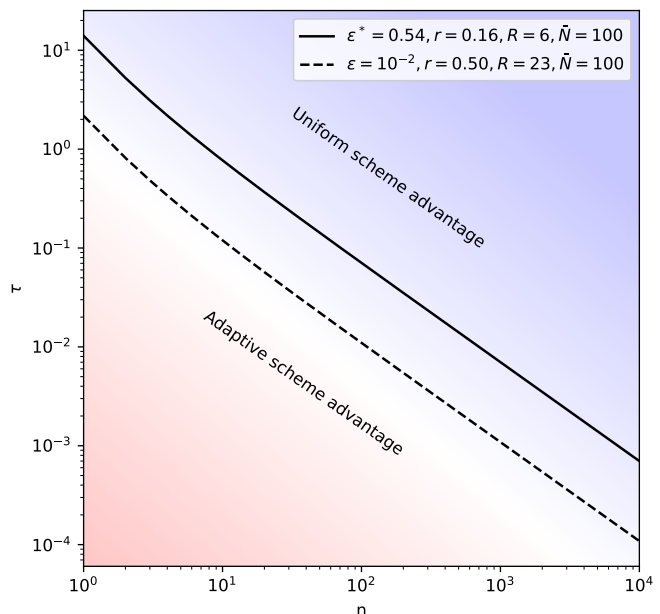


Fig. 4: Critical values of the relative cost parameter τ obtained from the condition $C_{\text{adaptive}}/C_{\text{uniform}} = 1$ as a function of the training data size. Each curve corresponds to a different choice of stopping threshold ε , effective shot fraction r , and number of adaptive rounds R . The curves separate two regimes: below a curve, the adaptive allocation is more cost-efficient than the uniform strategy; above it, the uniform scheme is cheaper. Regions close to the curves indicate parameter settings for which the two approaches have comparable total cost.

strategy favorable. For $\tau > \tau^*$, the classical cost dominates and uniform sampling becomes more efficient.

In typical quantum machine learning settings, the cost of quantum measurements is substantially higher than that of classical computation, implying small values of τ . At the same time, practical applications often involve moderate dataset sizes ($n \approx 10^1$ – 10^3). In this regime, the corresponding critical values τ^* tend to be significantly larger than realistic values of τ , placing most practical scenarios deep in the adaptive-advantage region.

Consequently, the adaptive measurement scheme offers a dual benefit: it not only improves the accuracy of the learned classifier, as demonstrated in the previous sections, but also reduces overall computational cost by exploiting early stopping and concentrating measurements on the most informative kernel entries.

V. NUMERICAL RESULTS AND DISCUSSION

In this section, we present the empirical evaluation of the proposed adaptive measurement strategy, examining its behavior under fixed-budget conditions, its performance when equipped with early stopping, and its sensitivity to key hyperparameters. We further relate these findings to the quantum–classical cost model, providing a unified interpretation of adaptive measurement efficiency under practical resource constraints.

A. Experimental Setup and Metrics

We evaluate the proposed adaptive measurement strategy on both synthetic and application-driven kernel settings. Synthetic datasets are generated from Gaussian mixture models with controllable structure, and kernel matrices are constructed using radial basis function (RBF) kernels. In addition, we consider simulated quantum kernel matrices obtained from real-world data, using feature maps based on block-encoding embeddings applied to the Indian Pines hyperspectral dataset for crop classification [18]. These kernels correspond to quantum circuits of varying size, ranging from 2 to 100 qubits, providing a realistic spectrum of kernel structures and noise sensitivities. Unless stated otherwise, results are averaged over 1000 independent runs.

a) Evaluation Metrics: We assess performance using several complementary measures:

Kernel reconstruction. We measure the root-mean-square error between the true and estimated kernel,

$$\text{RMSE}(K) = \sqrt{\frac{1}{n^2} \sum_{i,j} (K_{ij} - \hat{K}_{ij})^2},$$

as well as a support-vector-restricted variant $\text{RMSE}(K_{\text{SV}})$ focusing on entries involving true support vectors.

Support-vector recovery. We quantify agreement between true and estimated support-vector sets using the Jaccard index and a weighted variant based on the signed dual coefficients.

Classifier geometry. We measure the relative margin error and the decision-function RMSE, normalized by the true margin. These metrics quantify distortions in the separating hyperplane and deviations in decision values induced by kernel estimation noise.

In settings where a direct comparison between uniform and adaptive strategies is required, we additionally use the relative improvement metric

$$\Delta_{\text{RMSE}} = \frac{\text{RMSE}_f^{\text{uniform}} - \text{RMSE}_f^{\text{adaptive}}}{\text{RMSE}_f^{\text{uniform}}}, \quad (31)$$

which measures the reduction in decision-function error achieved by adaptive allocation relative to the uniform baseline. Positive values indicate that adaptive sampling yields lower error, while negative values correspond to regimes where uniform allocation performs better.

Unless otherwise noted, adaptive methods use a pilot stage followed by iterative refinement. We consider both fixed-budget scenarios, where all methods use the same total number of measurements, and early-stopping settings, where adaptive allocation may terminate before exhausting the budget.

B. Fixed-Budget Performance Experiments

The fixed-budget experiments reveal a consistent and pronounced advantage of the adaptive measurement scheme over the uniform baseline. Figure 5 summarizes the results across multiple metrics.

A key observation is that uniform allocation achieves lower global kernel reconstruction error, as measured by $\text{RMSE}(K)$, which is expected since it distributes measurements evenly

across all entries. However, this comes at the cost of poor accuracy in the most relevant parts of the kernel matrix. In particular, the SV-block RMSE shows that the adaptive strategy reconstructs interactions among true support vectors significantly more accurately. This improvement appears already after the first adaptive refinement round.

This behavior is consistent with the theoretical analysis in Sec. III, which predicts that only a subset of kernel entries contributes significantly to the SVM solution. By concentrating measurements on these entries, the adaptive scheme improves task-relevant accuracy rather than global kernel fidelity.

The advantage of adaptive allocation is further reflected in support-vector recovery. Both the Jaccard similarity and weighted Jaccard index demonstrate that the adaptive method more reliably identifies the true active set. The gap is particularly pronounced for the weighted Jaccard metric, indicating that adaptive sampling not only recovers the correct support vectors but also better captures their relative importance in the dual representation.

These improvements propagate directly to classifier-level performance. The adaptive scheme achieves substantially smaller errors in both relative margin and decision-function RMSE, indicating more accurate recovery of the separating hyperplane and decision values. Notably, these gains are immediate: adaptive sampling already outperforms uniform allocation after the first refinement round, and the advantage increases monotonically with subsequent rounds. This rapid improvement reflects the ability of the adaptive strategy to quickly focus measurement effort on the most informative kernel entries.

C. Adaptive convergence dynamics.

To better understand the behavior of the adaptive process, we examine its evolution over a larger number of rounds. Figure 6 shows the decision-function RMSE and dual-coefficient stability across up to fifty adaptive rounds.

The decision-function RMSE decreases monotonically, with a characteristic two-phase behavior. In the initial phase, the method exhibits rapid improvement, with a sharp reduction in error during the first several rounds. This is followed by a plateau phase, in which additional measurements yield diminishing returns. This saturation behavior indicates that most of the performance gain is achieved early in the adaptive process.

A closely matching trend is observed in the dual-coefficient stability measure. Large changes occur during the initial improvement phase, followed by stabilization as the RMSE curve flattens. Importantly, while RMSE requires access to the true kernel and is therefore not available during execution, the dual-stability metric is fully observable. Its convergence thus provides a practical and theoretically grounded stopping signal.

Taken together, these results demonstrate that adaptive measurement rapidly converges toward the true-kernel solution, and that most of the benefit can be obtained using only a small number of refinement rounds. This observation motivates the early-stopping strategy analyzed in the following subsection.

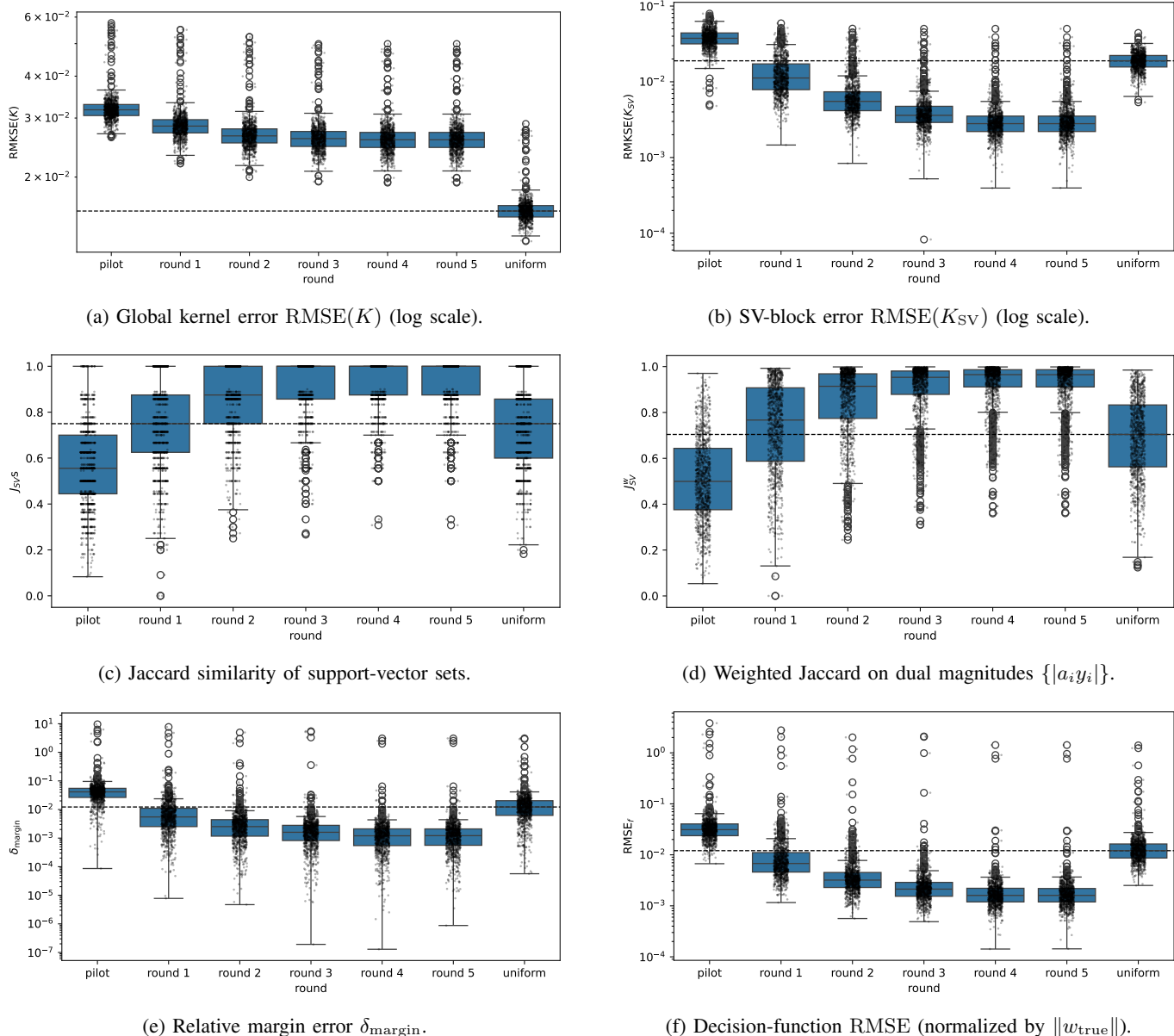


Fig. 5: Summary of metrics comparing *uniform* and *adaptive* measurement schemes across the algorithm stages (pilot, round 1, ..., round R). **Row 1:** Global kernel reconstruction error $\text{RMSE}(K)$ and SV-block error $\text{RMSE}(K_{SV})$, both on a logarithmic scale. **Row 2:** Support-vector set agreement (Jaccard, J_{SV}) and dual-weighted agreement (Weighted Jaccard, J_{SV}^w). **Row 3:** Relative margin error δ_{margin} and decision-function RMSE_f normalized by the true margin. Horizontal lines show the median of the uniform baseline. Support-vector indices correspond to the SVM trained on the true kernel K .

D. Early-Stopping Experiments

The early-stopping experiments evaluate whether the adaptive measurement procedure can terminate before exhausting the full budget while still achieving reliable model quality. The stopping rule is based on the dual-coefficient stability introduced in Eq. 29, which measures the relative change of the signed dual vector across consecutive rounds. Since this quantity is fully observable during training, it provides a practical surrogate for tracking convergence of the classifier without requiring access to the true kernel.

To assess the effect of the stopping threshold ε , we sweep a wide range of values and evaluate both accuracy and mea-

surement cost. The primary comparison metric is the relative improvement in decision-function RMSE, Δ_{RMSE} , between adaptive and uniform schemes. Positive values indicate an advantage for adaptive allocation, while negative values indicate that uniform sampling performs better.

The results, shown in Fig. 7, reveal a clear trade-off controlled by ε . For large thresholds, the algorithm terminates early, using only a very small fraction of the measurement budget. In this regime, the adaptive scheme may underperform the uniform baseline due to insufficient refinement of the kernel. As the threshold decreases, the algorithm is allowed to run for more rounds, improving accuracy and eventually

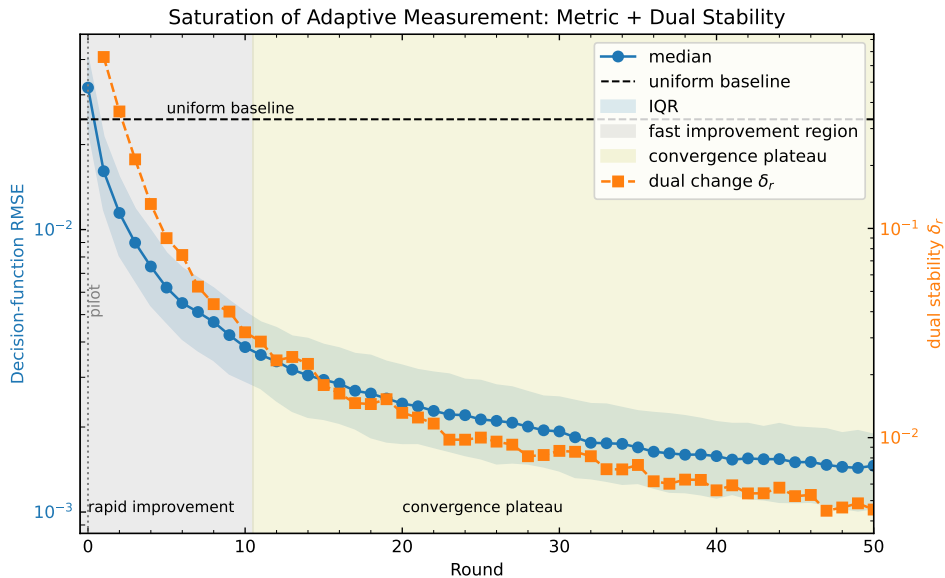


Fig. 6: Saturation behavior of the adaptive measurement scheme over 1000 random `make_blobs` datasets of 50 points. The blue curve shows the median decision–function RMSE across adaptive rounds, with an interquartile ribbon. A dashed horizontal line marks the performance of the uniform measurement baseline. The shaded region on the left highlights the phase of rapid improvement (pilot and early rounds), while the region on the right indicates the convergence plateau. The orange curve (right y -axis, log scale) displays the median dual–stability measure δ_r , showing that the SVM solution stabilizes as the adaptive kernel estimates converge.

surpassing uniform allocation.

A distinct transition occurs at a critical threshold $\varepsilon^* \approx 0.5$, where the sign of Δ_{RMSE} changes, indicating a regime in which adaptive allocation consistently outperforms uniform sampling. This transition is corroborated by the success-rate curve, which crosses approximately 50% at the same value, marking the boundary between the two regimes.

Beyond classification accuracy, Fig. 7 also quantifies measurement efficiency. At the critical threshold, the adaptive scheme uses only about 16% of the full shot budget and converges in a median of six rounds. This demonstrates a substantial reduction in measurement cost while maintaining competitive or superior performance. For smaller thresholds, the adaptive method achieves further improvements in accuracy while still using significantly fewer shots than the uniform baseline.

Overall, these results show that dual-coefficient stability provides an effective and practically implementable stopping criterion. It enables the adaptive scheme to identify the onset of the convergence plateau observed in Fig. 6, allowing early termination with minimal loss in accuracy. This yields a favorable trade-off between measurement cost and model quality, which is critical in resource-constrained quantum settings.

E. Regimes of dominance: uniform vs adaptive allocation

The theoretical analysis in Sec. III shows that the advantage of the optimal (oracle) allocation is governed by the heterogeneity of the weights w_{ij} . In practice, however, these weights must be estimated from noisy kernel measurements, which introduces additional uncertainty. This raises a key question:

in which regimes does adaptive allocation actually outperform uniform sampling?

To answer this, we perform a systematic exploration of data distributions that control the structure of the induced SVM solution. Synthetic datasets are generated from parametric Gaussian mixtures with tunable properties such as class separation, noise level, anisotropy, and label noise. These parameters directly affect the geometry of the decision boundary and, crucially, the sparsity of the dual coefficients.

To quantify the performance difference between the two strategies, we use the relative decision-function RMSE (defined in Eq.31) where positive values indicate that adaptive allocation improves over uniform sampling.

The results are summarized in Fig. 8. The horizontal axis measures the sparsity of the SVM solution via the Gini coefficient $G(\alpha)$, which quantifies how unevenly the dual coefficients are distributed: values close to zero correspond to nearly uniform coefficients, while larger values indicate that only a small subset of points (support vectors) carry significant weight. The vertical axis captures the normalized margin strength, reflecting class separation relative to data spread. Together, these quantities characterize the structural properties determining kernel heterogeneity.

Two distinct regimes emerge:

- **Low-structure regime (small $G(\alpha)$).** In this regime, the dual coefficients are broadly distributed and the weights w_{ij} are nearly uniform. Consequently, the oracle-optimal allocation offers little advantage over uniform sampling. Moreover, because adaptive allocation relies on noisy estimates of these nearly flat weights, estimation errors can dominate, leading to suboptimal measurement allocation.

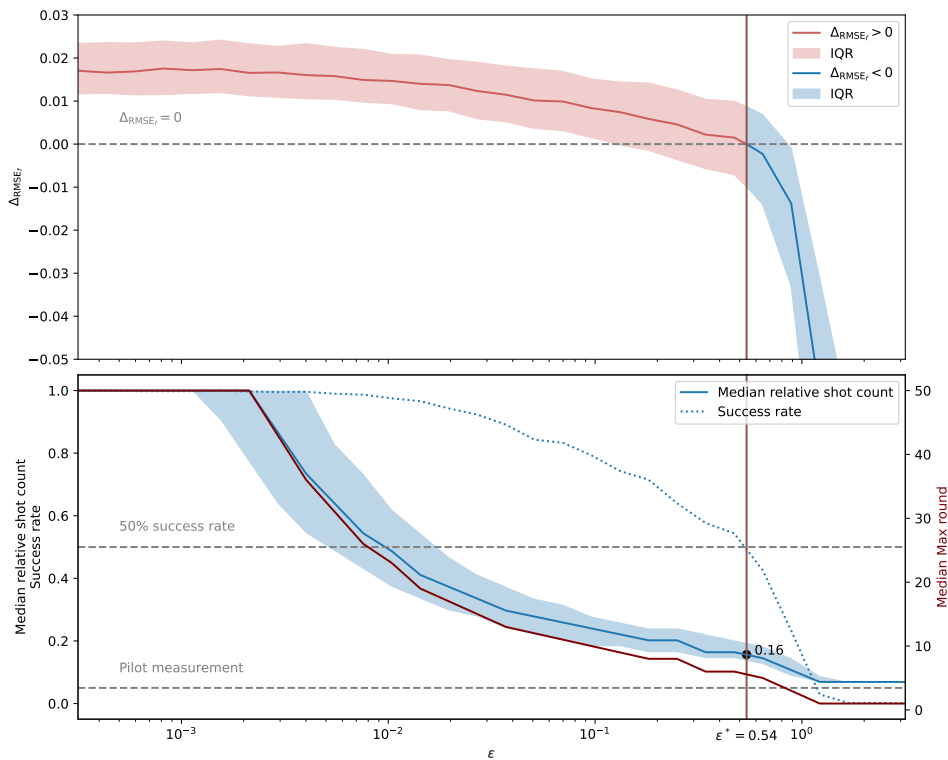


Fig. 7: Early stopping via dual-stability. The adaptive algorithm halts once the dual-stability change δ_* drops below a threshold ϵ . *Top*: Difference in decision-function RMSE between adaptive and uniform schemes (positive values indicate better adaptive performance). *Bottom*: Median relative shot count, success rate, and median number of rounds (right y -axis) as functions of ϵ , each computed over 1000 trials. The vertical line marks the critical ϵ separating the regimes in which adaptive or uniform sampling dominates.

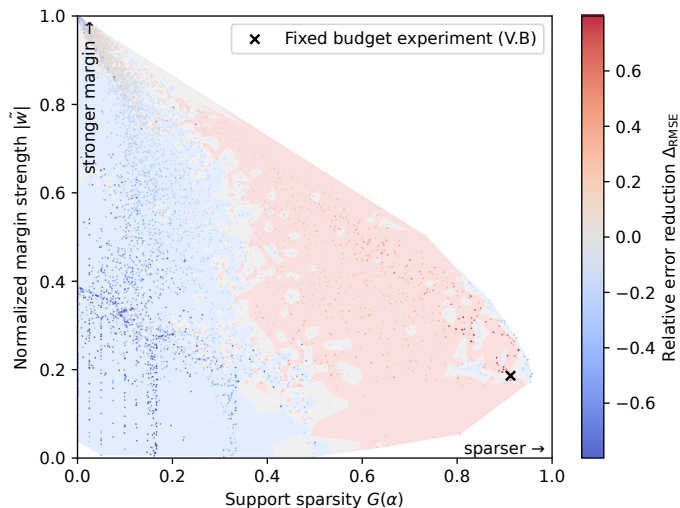


Fig. 8: Relative decision-function error reduction Δ_{RMSE} for adaptive vs uniform allocation across problem regimes. Each point corresponds to an average over 100 dataset realizations generated with varying structure parameters. Positive values indicate advantage of adaptive allocation, while negative values indicate that uniform sampling perform. The black cross indicates the location of the reference dataset used in previous experiments analysed in Sec.V-B.

As predicted by Proposition 2, uniform sampling can therefore match or even outperform adaptive strategies due to its robustness.

- **High-structure regime (large $G(\alpha)$ and strong margin).** Here, the SVM solution is sparse and the weights w_{ij} are highly heterogeneous. A small subset of kernel entries carries most of the influence on the classifier. Adaptive allocation exploits this structure by concentrating measurements on these influential entries, resulting in a substantial reduction in decision-function error relative to uniform sampling.

These results provide a direct empirical validation of the theoretical predictions: the effectiveness of adaptive allocation is governed by the heterogeneity of the underlying optimization landscape. In highly structured problems, adaptivity yields significant gains, while in near-homogeneous settings its advantage diminishes or disappears due to estimation noise.

The transition between these regimes aligns closely with the behavior observed in Fig. 2, where the dispersion of the weights w_{ij} controls the advantage of structured allocation. This confirms that heterogeneity is the key quantity governing both the theoretical and practical performance of adaptive measurement strategies.

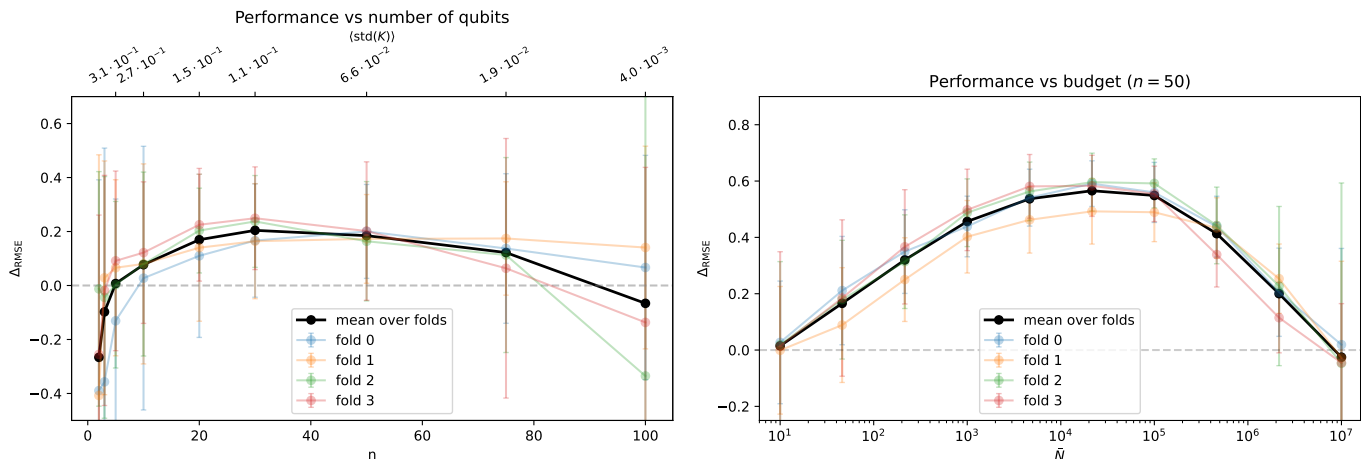


Fig. 9: Adaptive vs uniform measurement allocation on quantum kernels derived from the Indian Pines dataset using block-encoding feature maps. **Left:** Relative decision-function error reduction Δ_{RMSE} as a function of the number of qubits. The top axis shows the mean standard deviation of the independent kernel entries (averaged over folds), serving as a proxy for kernel concentration issue. Three regimes are visible: (i) a low-structure regime at small qubit numbers where uniform sampling performs slightly better, (ii) an intermediate regime with increased kernel variability where adaptive allocation achieves substantial gains, and (iii) a high-qubit regime where kernel concentration reduces effective signal and both methods exhibit comparable performance. **Right:** Relative error reduction as a function of the average number of shots per kernel entry, \bar{N} . For small budgets, both methods are dominated by measurement noise. At intermediate budgets, uniform allocation benefits from its robustness and broad coverage, while at large budgets both approaches converge as the kernel is accurately reconstructed. Results are averaged over four folds of the dataset. Positive values of Δ_{RMSE} indicate an advantage of adaptive allocation, while negative values correspond to superior performance of uniform sampling.

F. Adaptive Allocation for Quantum Kernels

To assess the behavior of the proposed method in realistic quantum machine learning settings, we evaluate adaptive and uniform allocation strategies on quantum kernels derived from the Indian Pines hyperspectral dataset. The kernels are generated using block-encoding feature maps, with system sizes ranging from 2 to 100 qubits, providing a controlled setting to study the interplay between kernel structure, measurement noise, and resource constraints.

Figure 9 summarizes the results. On the left, we report the relative decision-function error reduction Δ_{RMSE} as a function of the number of qubits, together with the mean standard deviation of kernel entries. On the right, we show the same metric as a function of the average measurement budget per kernel entry, \bar{N} .

The left panel reveals a clear three-regime behavior as the number of qubits increases. In the low-qubit regime, uniform allocation performs comparably to, and in some cases slightly better than, the adaptive strategy. Although the empirical variance of individual kernel entries is relatively high in this regime, this variability does not induce meaningful structure in the learning problem. The resulting SVM solutions are diffuse, with broadly distributed dual coefficients and weakly differentiated support vectors, leading to an effectively uniform sensitivity profile across kernel entries. As a result, targeted allocation provides limited advantage over uniform sampling.

In the intermediate regime, corresponding to moderate qubit numbers, a pronounced transition occurs. The kernel begins to induce a more structured decision geometry, and the SVM so-

lution becomes increasingly localized, with a clear separation of influential support vectors and a heterogeneous distribution of effective weights w_{ij} . In this setting, adaptive allocation significantly outperforms uniform sampling by concentrating measurements on the most informative kernel entries, leading to substantially improved decision-function accuracy. This regime aligns closely with the conditions identified in Sec. III, where heterogeneity in the induced importance weights enables strong gains from structured allocation.

For larger system sizes, the kernel enters a regime dominated by concentration effects [5], in which off-diagonal entries shrink and the effective signal available for classification diminishes. In this setting, both methods experience a degradation in performance under a fixed measurement budget, and their performance becomes comparable. However, adaptive allocation remains valuable in practice, as it enables more efficient use of limited resources and allows exploration of deeper concentration regimes before performance collapses. While it does not eliminate the impact of kernel concentration, it extends the range of system sizes for which meaningful learning remains feasible.

The right panel examines the dependence of performance on the measurement budget for a fixed system size (50 qubits). For very small budgets, both methods perform similarly, as the available measurements are insufficient to reliably estimate the kernel structure, and estimation noise dominates. As the budget increases, a clear performance gap emerges: adaptive allocation significantly outperforms uniform sampling by focusing resources on the most informative kernel entries,

leading to substantially lower decision-function error. In the large-budget regime, the gap closes as both methods approach the ideal classifier, with sufficient measurements to accurately reconstruct the kernel regardless of the allocation strategy.

Taken together, these results demonstrate that the effectiveness of adaptive measurement depends on both the structure of the kernel and the available measurement budget. While its benefits are limited in regimes where the learning problem lacks structure or where the signal is fundamentally degraded by concentration, adaptive allocation provides substantial gains in the practically relevant intermediate regime and remains effective over a broad range of budgets. In particular, it enables more efficient use of measurement resources and extends the operating regime of kernel-based learning beyond what is achievable with uniform sampling alone.

VI. CONCLUSION

In this work, we studied the problem of learning kernelized Support Vector Machines under measurement constraints, where the kernel matrix must be estimated from noisy observations and the learner controls accuracy through the allocation of a limited measurement budget. We showed that uniform allocation, while statistically balanced, fails to exploit the highly non-uniform dependence of the SVM solution on the Gram matrix.

To address this, we introduced an adaptive measurement-allocation strategy that is explicitly guided by the structure of the SVM problem. Our approach combines geometric sensitivity, capturing the influence of individual kernel entries on the margin, with active-set instability, quantifying the probability of discrete changes in support-vector membership. These complementary signals enable a task-aware allocation scheme that concentrates measurement effort on the most decision-critical regions of the kernel.

On the theoretical side, we demonstrated that the advantage of adaptive allocation is governed by the heterogeneity of the induced kernel importance structure. This leads to a clear regime-dependent picture: in strongly structured problems, adaptive allocation provides substantial gains, while in near-homogeneous settings its benefits diminish due to estimation noise. On the algorithmic side, we developed a multi-round adaptive procedure with an early-stopping criterion based on dual-coefficient stability, allowing the method to terminate once the classifier has effectively converged. Experimentally, we showed that this approach improves support-vector recovery, margin estimation, and decision-function accuracy under fixed budgets, while often requiring only a fraction of the measurements.

Beyond synthetic evaluations, experiments on quantum kernels derived from real-world data revealed a consistent interplay between kernel structure, measurement budget, and system size. In particular, adaptive allocation is most effective in intermediate regimes where the kernel induces a structured and heterogeneous SVM solution, leading to substantial improvements in decision-function accuracy. While performance degrades in regimes dominated by kernel concentration or severe measurement noise, adaptive allocation continues to

make more efficient use of the available measurement budget and extends the range of conditions under which meaningful learning remains feasible. This connection highlights the relevance of the proposed method for quantum machine learning, where measurement efficiency and kernel degradation are central challenges.

Overall, our results establish adaptive, sensitivity-driven measurement allocation as a principled and effective alternative to uniform sampling for learning with noisy kernels, offering improvements in both predictive performance and computational efficiency.

Several directions for future work remain open. First, extending the theoretical analysis of active-set instability, for example through sharper characterizations of transition probabilities, could further clarify the role of uncertainty in structured learning problems. Second, incorporating more realistic hardware noise models, including time-correlated and device-specific effects, would strengthen the connection to practical quantum implementations. Finally, exploring extensions of the proposed framework to other kernel methods [19] and learning paradigms, as well as integrating it with complementary techniques such as kernel approximation or compression, presents promising avenues for improving scalability in measurement-limited settings.

REFERENCES

- [1] T. Hofmann, B. Schölkopf, and A. J. Smola, “Kernel methods in machine learning,” *The Annals of Statistics*, vol. 36, no. 3, pp. 1171 – 1220, 2008. [Online]. Available: <https://doi.org/10.1214/009053607000000677>
- [2] V. Havlíček, A. D. Córcoles, K. Temme, A. W. Harrow, A. Kandala, J. M. Chow, and J. M. Gambetta, “Supervised learning with quantum-enhanced feature spaces,” *Nature*, vol. 567, no. 7747, pp. 209–212, 2019.
- [3] M. Schuld and N. Killoran, “Quantum machine learning in feature hilbert spaces,” *Physical review letters*, vol. 122, no. 4, p. 040504, 2019.
- [4] J. R. McClean, S. Boixo, V. N. Smelyanskiy, R. Babbush, and H. Neven, “Barren plateaus in quantum neural network training landscapes,” *Nature Communications*, vol. 9, no. 1, p. 4812, Nov. 2018.
- [5] S. Thanasilp, S. Wang, M. Cerezo, and Z. Holmes, “Exponential concentration in quantum kernel methods,” *Nature Communications*, vol. 15, no. 1, p. 5200, 2024.
- [6] A. Miroszewski, M. F. Asiani, J. Mielczarek, B. L. Saux, and J. Nalepa, “In search of quantum advantage: Estimating the number of shots in quantum kernel methods,” 2024. [Online]. Available: <https://arxiv.org/abs/2407.15776>
- [7] G. Gentinetta, A. Thomsen, D. Sutter, and S. Woerner, “The complexity of quantum support vector machines,” *Quantum*, vol. 8, p. 1225, 2024.
- [8] R. Coelho, G. Kruse, and A. Rosskopf, “Quantum-efficient kernel target alignment,” *arXiv preprint arXiv:2502.08225*, 2025.
- [9] A. Naveh, I. Fitzgerald, A. Phan, A. Lockwood, and T. L. Scholten, “Kernel matrix completion for offline quantum-enhanced machine learning,” *arXiv preprint arXiv:2112.08449*, 2021.
- [10] A. Shastry, A. Jayakumar, A. Patel, and C. Bhattacharyya, “Shot-frugal and robust quantum kernel classifiers,” *arXiv preprint arXiv:2210.06971*, 2022.
- [11] J. Xu, C. Li, D. Zeng, J. Paisley, and Q. Zhao, “Aqka: Active quantum kernel acquisition under a shot budget,” *arXiv preprint arXiv:2605.14672*, 2026.
- [12] E. Gil-Fuster, S. Shin, S. Jerbi, J. Eisert, and M. J. Kramer, “Optimal algorithmic complexity of inference in quantum kernel methods,” *arXiv preprint arXiv:2604.15214*, 2026.
- [13] J. Preskill, “Quantum computing in the NISQ era and beyond,” *Quantum*, vol. 2, p. 79, 2018.
- [14] M. Vukšić, J. Čelić, and A. Cuculić, “Comparative analysis of contemporary quantum computer processors: Architectures, performance and perspectives,” *IEEE access*, 2026.

- [15] A. Javadi-Abhari, M. Treinish, K. Krsulich, C. J. Wood, J. Lishman, J. Gacon, S. Martiel, P. D. Nation, L. S. Bishop, A. W. Cross *et al.*, “Quantum computing with Qiskit,” *arXiv preprint arXiv:2405.08810*, 2024.
- [16] V. Bergholm, J. Izaac, M. Schuld, C. Gogolin, S. Ahmed, V. Ajith, M. S. Alam, G. Alonso-Linaje, B. AkashNarayanan, A. Asadi *et al.*, “PennyLane: Automatic differentiation of hybrid quantum-classical computations,” *arXiv preprint arXiv:1811.04968*, 2018.
- [17] C.-C. Chang and C.-J. Lin, “Libsvm: A library for support vector machines,” *ACM transactions on intelligent systems and technology (TIST)*, vol. 2, no. 3, pp. 1–27, 2011.
- [18] A. Delilbasic, A. Miroszewski, A. Wijata, J. Nalepa, J. Mielczarek, M. Riedel, and G. Cavallaro, “Large-Scale Quantum Kernels for Hyperspectral Data Classification,” 2026. [Online]. Available: <https://arxiv.org/abs/2605.17587>
- [19] J. Jäger, P. Braccia, P. Bermejo, M. G. Algaba, D. García-Martín, and M. Cerezo, “Provable and scalable quantum gaussian processes for quantum learning,” *arXiv preprint arXiv:2605.00099*, 2026.

APPENDIX A

VARIANCE OF KERNEL ESTIMATES UNDER HARDWARE AND SAMPLING NOISE

In this appendix we derive the expectation and variance of the empirical kernel estimator in the presence of both sampling noise and stochastic hardware-induced fluctuations.

A. Model Definition

We consider a fixed kernel entry (i, j) and omit indices for clarity. Let

$$K \in [0, 1] \quad (32)$$

denote the true kernel value.

We assume that each execution of the kernel evaluation procedure produces an *effective* kernel realization

$$\tilde{K}^{(t)} = K + \varepsilon^{(t)}, \quad (33)$$

where the noise process $\{\varepsilon^{(t)}\}_{t=1}^N$ satisfies

$$\mathbb{E}[\varepsilon^{(t)}] = 0, \quad (34)$$

and is not necessarily independent across different measurements. In particular, we allow

$$\text{Cov}(\varepsilon^{(t)}, \varepsilon^{(s)}) \neq 0 \quad \text{for } t \neq s. \quad (35)$$

Given a realization $\tilde{K}^{(t)}$, the observed measurement is

$$X^{(t)} \sim \text{Bernoulli}(\tilde{K}^{(t)}), \quad (36)$$

and we define the empirical estimator

$$\hat{K} = \frac{1}{N} \sum_{t=1}^N X^{(t)}. \quad (37)$$

B. Expectation of the Estimator

We compute the expectation using the law of total expectation:

$$\mathbb{E}[X^{(t)}] = \mathbb{E}[\mathbb{E}[X^{(t)} | \tilde{K}^{(t)}]] \quad (38)$$

$$= \mathbb{E}[\tilde{K}^{(t)}] \quad (39)$$

$$= K. \quad (40)$$

Therefore,

$$\mathbb{E}[\hat{K}] = \frac{1}{N} \sum_{t=1}^N \mathbb{E}[X^{(t)}] = K. \quad (41)$$

Thus, the estimator \hat{K} is unbiased for the true kernel value.

C. Variance of the Estimator

We compute the variance of \hat{K} :

$$\text{Var}(\hat{K}) = \text{Var}\left(\frac{1}{N} \sum_{t=1}^N X^{(t)}\right). \quad (42)$$

Using the standard variance decomposition for sums,

$$\text{Var}(\hat{K}) = \frac{1}{N^2} \left(\sum_{t=1}^N \text{Var}(X^{(t)}) + \sum_{t \neq s} \text{Cov}(X^{(t)}, X^{(s)}) \right). \quad (43)$$

1) *Variance of Individual Measurements:* We apply the law of total variance:

$$\text{Var}(X^{(t)}) = \mathbb{E}[\text{Var}(X^{(t)} | \tilde{K}^{(t)})] + \text{Var}(\mathbb{E}[X^{(t)} | \tilde{K}^{(t)}]). \quad (44)$$

Since

$$\text{Var}(X^{(t)} | \tilde{K}^{(t)}) = \tilde{K}^{(t)}(1 - \tilde{K}^{(t)}), \quad (45)$$

$$\mathbb{E}[X^{(t)} | \tilde{K}^{(t)}] = \tilde{K}^{(t)}, \quad (46)$$

we obtain

$$\text{Var}(X^{(t)}) = \mathbb{E}[\tilde{K}^{(t)}(1 - \tilde{K}^{(t)})] + \text{Var}(\tilde{K}^{(t)}). \quad (47)$$

Using the identity

$$\mathbb{E}[\tilde{K}(1 - \tilde{K})] = K(1 - K) - \text{Var}(\tilde{K}), \quad (48)$$

we obtain

$$\text{Var}(X^{(t)}) = K(1 - K). \quad (49)$$

2) *Covariance Between Measurements:* We compute the covariance using the law of total covariance:

$$\text{Cov}(X^{(t)}, X^{(s)}) = \mathbb{E}[\text{Cov}(X^{(t)}, X^{(s)} | \tilde{K})] + \text{Cov}(\mathbb{E}[X^{(t)} | \tilde{K}], \mathbb{E}[X^{(s)} | \tilde{K}]), \quad (50)$$

Given $\tilde{K}^{(t)}$ and $\tilde{K}^{(s)}$, the measurements are conditionally independent, hence

$$\text{Cov}(X^{(t)}, X^{(s)} | \tilde{K}) = 0. \quad (51)$$

Therefore,

$$\text{Cov}(X^{(t)}, X^{(s)}) = \text{Cov}(\tilde{K}^{(t)}, \tilde{K}^{(s)}). \quad (52)$$

We define

$$\sigma_{\text{phys}}^2 := \text{Cov}(\tilde{K}^{(t)}, \tilde{K}^{(s)}), \quad t \neq s, \quad (53)$$

which captures the contribution of correlated hardware-induced fluctuations.

3) *Final Expression:* We now combine the results:

$$\text{Var}(\hat{K}) = \frac{1}{N^2} (NK(1 - K) + N(N - 1)\sigma_{\text{phys}}^2) \quad (54)$$

$$= \frac{K(1 - K)}{N} + \left(1 - \frac{1}{N}\right) \sigma_{\text{phys}}^2. \quad (55)$$

D. Discussion

The variance of the kernel estimator decomposes into two contributions:

- A *sampling (shot) noise* term, $\frac{K(1-K)}{N}$, which decreases with the number of measurements.
- An *irreducible hardware-induced term*, $(1 - \frac{1}{N})\sigma_{\text{phys}}^2$, which arises from correlations between kernel realizations across measurements.

In particular,

$$\lim_{N \rightarrow \infty} \text{Var}(\widehat{K}) = \sigma_{\text{phys}}^2, \quad (56)$$

showing that correlated fluctuations of the effective kernel impose a fundamental limit on the precision of kernel estimation that cannot be overcome by increasing the number of measurements.

APPENDIX B

MARGIN SENSITIVITY VIA THE ENVELOPE THEOREM

In Sec. II-C we use the fact that, when a perturbation of a kernel entry K_{ij} does not alter the active set of support vectors, the derivative of the squared margin with respect to K_{ij} can be computed without differentiating through the optimal dual variables $\alpha^*(K)$. This appendix provides a concise justification based on the envelope theorem.

Recall the SVM dual objective:

$$\max_{\alpha \in \mathcal{A}} g(\alpha, K), \quad (57)$$

with

$$g(\alpha, K) = \sum_{i=1}^n \alpha_i - \frac{1}{2} \sum_{i,j=1}^n \alpha_i \alpha_j y_i y_j K_{ij}, \quad (58)$$

and feasible set

$$\mathcal{A} = \left\{ 0 \leq \alpha_i \leq C, \sum_i \alpha_i y_i = 0 \right\}.$$

For fixed kernel K , let $\alpha^*(K)$ denote the unique optimal solution (on the active-set manifold). Define the optimal dual value:

$$V(K) = g(\alpha^*(K), K). \quad (59)$$

The (Milgrom–Segal) envelope theorem states that, if $V(K) = \max_{\alpha \in \mathcal{A}} g(\alpha, K)$ and the maximizer $\alpha^*(K)$ varies smoothly in a neighborhood where the active set of constraints does not change, then

$$\frac{\partial V(K)}{\partial K_{ij}} = \left. \frac{\partial g(\alpha, K)}{\partial K_{ij}} \right|_{\alpha = \alpha^*(K)}. \quad (60)$$

Intuitively, when α^* is the optimizer for the current K , the directional derivative of g in any feasible tangent direction is already zero (first-order KKT stationarity). Therefore the only “direct” sensitivity at optimum comes from the explicit dependence of the objective on K , not from the optimizer’s movement.

APPENDIX C

OPTIMAL MEASUREMENT ALLOCATION

A. General Allocation Principle

Consider the optimization problem

$$\min_{\{N_{ij}\}} \sum_{i < j} \frac{w_{ij}}{N_{ij}} \quad \text{s.t.} \quad \sum_{i < j} N_{ij} = N_{\text{tot}}, \quad N_{ij} > 0, \quad (61)$$

where $w_{ij} \geq 0$ are arbitrary weights.

The Lagrangian is given by

$$\mathcal{L} = \sum_{i < j} \frac{w_{ij}}{N_{ij}} + \lambda \left(\sum_{i < j} N_{ij} - N_{\text{tot}} \right). \quad (62)$$

Differentiating with respect to N_{ij} yields

$$-\frac{w_{ij}}{N_{ij}^2} + \lambda = 0, \quad (63)$$

which implies

$$N_{ij} = \sqrt{\frac{w_{ij}}{\lambda}}. \quad (64)$$

Imposing the constraint gives

$$\sum_{i < j} \sqrt{\frac{w_{ij}}{\lambda}} = N_{\text{tot}}, \quad (65)$$

hence

$$\sqrt{\lambda} = \frac{\sum_{i < j} \sqrt{w_{ij}}}{N_{\text{tot}}}. \quad (66)$$

Substituting back, we obtain the general solution

$$N_{ij}^* = N_{\text{tot}} \frac{\sqrt{w_{ij}}}{\sum_{k < l} \sqrt{w_{kl}}}. \quad (67)$$

B. Margin Variance Minimization

Using first-order sensitivity analysis, the variance of the squared margin can be approximated as

$$V_{\text{margin}} = \sum_{i < j} (\alpha_i \alpha_j)^2 \frac{K_{ij}(1 - K_{ij})}{N_{ij}}. \quad (68)$$

This corresponds to weights

$$w_{ij}^{\text{margin}} := (\alpha_i \alpha_j)^2 K_{ij}(1 - K_{ij}). \quad (69)$$

Substituting into the general solution yields

$$N_{ij}^{\text{margin}} \propto |\alpha_i \alpha_j| \sqrt{K_{ij}(1 - K_{ij})}. \quad (70)$$

C. Decision Function Variance Minimization

The variance of the decision function is given by

$$\sigma_{f,i}^2 = \sum_j (\alpha_j y_j)^2 \frac{K_{ij}(1 - K_{ij})}{N_{ij}}. \quad (71)$$

Summing over i yields

$$V_{\text{dec}} = \sum_{i < j} (\alpha_i^2 + \alpha_j^2) \frac{K_{ij}(1 - K_{ij})}{N_{ij}}, \quad (72)$$

which corresponds to weights

$$w_{ij}^{\text{dec}} := (\alpha_i^2 + \alpha_j^2) K_{ij}(1 - K_{ij}). \quad (73)$$

Applying the general solution gives

$$\boxed{N_{ij}^{\text{dec}} \propto \sqrt{\alpha_i^2 + \alpha_j^2} \sqrt{K_{ij}(1 - K_{ij})}.} \quad (74)$$

D. Comparison of Allocation Strategies

Both allocation schemes share the same functional form and differ only in the dependence on the dual variables:

$$N_{ij}^{\text{margin}} \propto |\alpha_i \alpha_j|, \quad (75)$$

$$N_{ij}^{\text{dec}} \propto \sqrt{\alpha_i^2 + \alpha_j^2}. \quad (76)$$

Using the inequalities

$$|\alpha_i \alpha_j| \leq \frac{\alpha_i^2 + \alpha_j^2}{2}, \quad (77)$$

it follows that the two allocation strategies are equivalent up to multiplicative constants.

In particular, both concentrate measurement effort on pairs involving data points with large dual coefficients, i.e., on support vectors.

APPENDIX D PROPOSITION PROOFS

A. Proposition 1

The proof follows the obtained variances

$$V_{\text{unif}} = \frac{n(n-1)}{2N_{\text{tot}}} \sum_{i<j} w_{ij},$$

while the optimal allocation yields

$$V^* = \frac{(\sum_{i<j} \sqrt{w_{ij}})^2}{N_{\text{tot}}}.$$

and the Cauchy-Schwarz inequality,

$$\left(\sum_{i=1}^n u_i v_i \right)^2 \leq \left(\sum_{i=1}^n u_i^2 \right) \left(\sum_{i=1}^n v_i^2 \right).$$

We take the sum over all the independent matrix elements $\sum_{i<j} \equiv \sum_i$, take $u_i = \sqrt{w_{ij}}$, and $v_i = 1$. We get

$$\left(\sum_{i<j} \sqrt{w_{ij}} \cdot 1 \right)^2 \leq \left(\sum_{i=1}^n w_{ij} \right) \underbrace{\left(\sum_{i<j} 1 \right)}_{\frac{n(n-1)}{2}}.$$

Dividing both sides of the equation by N_{tot} , we get

$$V^* \leq V_{\text{unif}},$$

which finishes the proof.

B. Proposition 2

The variance objective is given by

$$V = \sum_{i<j} \frac{w_{ij}}{N_{ij}}.$$

Let N_{ij}^* denote the oracle-optimal allocation, and consider a perturbed allocation

$$N_{ij} = N_{ij}^* + \delta N_{ij},$$

subject to the constraint

$$\sum_{i<j} \delta N_{ij} = 0.$$

We perform a second-order Taylor expansion of the function $f(x) = 1/x$ around $x = N_{ij}^*$:

$$\frac{1}{N_{ij}} = \frac{1}{N_{ij}^*} - \frac{\delta N_{ij}}{(N_{ij}^*)^2} + \frac{(\delta N_{ij})^2}{(N_{ij}^*)^3} + \mathcal{O}((\delta N_{ij})^3).$$

Substituting this expansion into the expression for V , we obtain

$$V \approx \sum_{i<j} w_{ij} \left(\frac{1}{N_{ij}^*} - \frac{\delta N_{ij}}{(N_{ij}^*)^2} + \frac{(\delta N_{ij})^2}{(N_{ij}^*)^3} \right).$$

The first term recovers the optimal value:

$$V^* = \sum_{i<j} \frac{w_{ij}}{N_{ij}^*}.$$

The first-order term vanishes at the optimum. This follows from the first-order optimality (KKT) conditions for the constrained minimization problem, which ensure that the gradient of V at N^* is orthogonal to feasible perturbations satisfying $\sum_{i<j} \delta N_{ij} = 0$.

Thus, retaining terms up to second order,

$$V \approx V^* + \sum_{i<j} \frac{w_{ij}}{(N_{ij}^*)^3} (\delta N_{ij})^2.$$

Taking expectation and assuming that $\mathbb{E}[\delta N_{ij}] = 0$, we obtain

$$\mathbb{E}[V] = V^* + \sum_{i<j} \frac{w_{ij}}{(N_{ij}^*)^3} \mathbb{E}[(\delta N_{ij})^2] + \mathcal{O}(\|\delta N\|^3),$$

which completes the proof.

APPENDIX E HYPERPARAMETER SELECTION

We summarize the key parameters used in the adaptive measurement procedure.

- **Total measurement budget** N_{tot} . Determined by experimental constraints.
- **Number of adaptive rounds** R . Sets the maximum number of refinement iterations. Unless early stopping is triggered, the remaining budget after the pilot stage is distributed uniformly across the rounds.
- **Score weight** λ . Controls the balance between geometric sensitivity and active-set instability (Eq. 28). We use $\lambda = 0.5$.

- **Pilot shots** m_0 . Each kernel entry is initialized using m_0 measurements, with total cost

$$N_{\text{pilot}} = m_0 \cdot \frac{n(n-1)}{2}.$$

- **Stopping threshold** ε . The algorithm stops when $\delta_r < \varepsilon$. We consider values in the range 10^{-2} – 10^{-1} .
- **SVM regularization** C . Fixed throughout optimization; default values from standard libraries are used.